Journal of Marine Science and Technology

Volume 26 | Issue 3 Article 6

THE RESEARCH OF ADDED RESISTANCE IN WAVES BASED ON NONLINEAR TIME-DOMAIN POTENTIAL FLOW THEORY

Bao-Ji Zhang
College of Ocean Science and Engineering, Shanghai Maritime University, Shanghai, China., zbj1979@163.com

Xu- Ning
Merchant Marine College, Shanghai Maritime University, Shanghai, China.

THE RESEARCH OF ADDED RESISTANCE IN WAVES BASED ON NONLINEAR TIME-DOMAIN POTENTIAL FLOW THEORY

Acknowledgements

Foundation item: Supported by National P & D Program of China (No.2016YFB0300700, 2016YF0300704), National Natural Science Foundation of China (No. 51779135, 51009087), Shanghai Natural Science Foundation of China (project approval number: 14ZR1419500).

Journal of Marine Science and Technology, Vol. 26, No. 3, pp. 343-351 (2018)
DOI: 10.6119/JMST.2018.06_(3).0006

THE RESEARCH OF ADDED RESISTANCE IN WAVES BASED ON NONLINEAR TIME-DOMAIN POTENTIAL FLOW THEORY

Bao-Ji Zhang[1] and Xu-Ning[2]

Key words: added resistance in waves, three-dimensional fully nonlinear, time-domain analysis.

ABSTRACT

In order to accurately predict the motion performance of the ship in waves, the numerical calculation of heave, pitch and added resistance of a container ship in a regular wave is studied based on the three-dimensional fully nonlinear time-domain potential flow theory. The boundary element method is used to deal with the quadrilateral elements, and the governing equations are solved by the first-order flat-plate theory and the fourth-order Runge-Kutta time integration method. The ship hull is divided by the fixed mesh. Considering the non-linear superposition of the forward velocity, the stationary ship wave, diffracted wave, diffraction wave and incident wave field, the free surface is generated by the hybrid Euler-Lagrangian method, and the damping area is set manually at the edge. Take the KCS container ship for instance, the calculation results of heave, pitch and added resistance in waves are compared with the experimental values. The results show that the biggest advantage of this method is to get a more accurate prediction of ship motion in a short time, and this method has a broad application prospect in the analysis and motion prediction of ship hydrodynamic performance in waves.

I. INTRODUCTION

With the rapid development of shipping industry and the strengthening of environmental protection concept, the issue of energy conservation and emission reduction has been widely concerned in shipbuilding industry, more and more scholars began to research on ship energy conservation and emissions reduction, especially after the International Marine Organization (IMO) proposed the Energy Efficiency Design Index (EEDI). The study found that the ship with low resistance and good performance in still water cannot reach the ideal state under actual sea conditions, and there are different degrees of stalling, of which the added resistance in waves is the most important parameter affecting the stall factor. To this end, domestic and foreign experts and scholars carried out a large number of computation study of added resistance. Duan et al. (2014) solved the motion response and added resistance of high-speed craft in the regular and irregular waves basing on the 2.5-D theory and pressure integral method. Based on the 2-D slice theory and combined with Gerritsma and Beukelman energy radiation method, Li et al. (2012) calculated the added resistance of a bulk carrier and put forward that ships using vertical bow have better resistance performance in waves. Shen et al. (2012) adopted the RANS equation as the control equation and discretized by the finite volume method, and he used the VOF method to calculate the motion response and added resistance of the Wigley ship model. Jin et al. (2013) analyzed the added resistance of the ship in variable roll attitudes in accordance with the potential flow theory. Zhang (2011) proposed the multi-objective ship form optimization method, comprehensively considered the minimum of still water resistance and added resistance, and took S60 ship as an example to verify the feasibility of ship form optimization. Kim et al. (2011) used the Rankine source method and time-domain analysis method to forecast the added resistance of various ship types such as Wigley ship, S60HE ship, S175 container ship. Seo et al. (2013) comparatively studied the method for calculating added resistance in waves and calculated the added resistance by the slice method, the Rankine source method and the body-fitted grid method. Park et al. (2015) performed an uncertainty analysis of the motion response and added resistance of KVLCC2. Since the twenty-first century, with the rapid development of computer technology, computational fluid dynamics (CFD) has been widely used for the prediction of ship hydrodynamic performance. It has become a new method to solve the problem of added resistance in waves by establishing a three-dimensional numerical wave tank. Based on the CFD technology, Xie et al. (2013) and Xie et al. (2017) built a three-dimensional numerical wave tank by the Fluent software, and calculated the added resistance in waves of the high speed displacement-type ships. Deng et al. (2015) and Fang et al. (2012) also used 3-D numerical wave tank to simulate the effects of waves on ships, and calcu-

Paper submitted 04/11/17; revised 12/05/17; accepted 04/18/18. Author for correspondence: Bao-Ji Zhang (e-mail: zbj1979@163.com).
[1] College of Ocean Science and Engineering, Shanghai Maritime University, Shanghai, China.
[2] Merchant Marine College, Shanghai Maritime University, Shanghai, China.

lated the hydrodynamic performance of ships in head and oblique waves at different speeds. Fang et al. (2012) simulated generation and propagation of regular waves based on CFD, and calculated the numerical simulation of ship motion and added resistance in head sea.

In short, there are various theoretical methods for calculating the added resistance of the ship. Slice theory, 3-D linear time-domain method and partial nonlinear time-domain potential flow method are insufficient in accuracy, but these methods have a short computation time and the development are quite mature. Large-eddy simulation (LES), direct numerical simulation (DNS) and Reynolds average Navier Stokes (RANS) have high accuracy, but these methods have a long computation time. In contrast, 3-D fully nonlinear time-domain potential flow method is more accurate for simulating the free surface considering the feature of modern ship's bow flare. In the case of considering the computation time and computational accuracy, the method is more reasonable to calculate the added resistance of the ship. Therefore, in this paper, basing on the results of previous studies and 3-D fully nonlinear time-domain potential flow theory, we used Shipflow software and self-compiled program to calculate heave, pitch and added resistance of a container ship at the speed of Fr = 0.26 in regular waves of the λ/L (wave length-ship length ratio) = 0.5~2, A_K = 1/60.

II THEORETICAL BASIS

1. Potential Flow Theory

On the basis of the potential flow assumption, the flow is assumed to be nonviscous, incompressible and irrotational. Therefore, there exists a velocity potential function, which satisfies the Laplace equation in the fluid region.

$$\nabla^2\phi = 0 \tag{1}$$

1) Computational Domain

The computational domain consists of a free surface and a hull, assuming that it is part of a larger computational domain of known conditions, and the external computational domain is a still water or free-interference incident wave domain.

2) Boundary Conditions

On the free surface, the velocity potential satisfies the motion and dynamic boundary conditions.

$$\frac{D\vec{x}}{Dt} = \nabla\phi \tag{2}$$

$$\frac{D\phi}{Dt} = -gz + \frac{1}{2}\nabla\phi\cdot\nabla\phi - \frac{P_a}{\rho} \tag{3}$$

where $\vec{x} = (x, y, z)$ is the coordinates of the point on the free surface, and P_a is atmospheric pressure. The material derivative is defined as

$$\frac{D}{Dt} = \frac{\partial}{\partial t} + \nabla\phi\cdot\nabla \tag{4}$$

On the hull surface, an impermeable boundary condition is applied, i.e.,

$$\frac{\partial\phi}{\partial n} = \vec{n}\cdot\left(\vec{u} + \vec{\omega}\times\vec{\gamma}'\right) \tag{5}$$

where $\vec{n}$ is the vertical component of the hull surface, $\vec{u}$ and $\vec{\omega}$ are the linear velocity and angular velocity of the hull, $\vec{r}'$ is the radial velocity of the rotation center.

3) Hydrodynamic Pressure and Hydrodynamic Force Calculation

The Bernoulli equation is used to solve the unsteady hydrodynamic pressure of any point in the computational domain, i.e.,

$$p = -\rho\left(\frac{\partial\phi}{\partial t} + \frac{1}{2}\left|\nabla\phi\right|^2 + gz\right) \tag{6}$$

The partial derivative of velocity potential respect to time is

$$\frac{\partial\phi}{\partial t} = \frac{d\phi}{dt} - \vec{v}'\cdot\nabla\phi \tag{7}$$

where $\vec{v}'$ is the velocity of the solution point.

The hydrodynamic force and bending moment of the hull are obtained by integrating along the wet surface, i.e.,

$$\vec{F} = -\iint_{S_b} p\vec{n}dS \tag{8}$$

$$\vec{M} = -\iint_{S_b} p\left(\vec{\gamma}'\times\vec{n}\right)dS \tag{9}$$

where

$$\vec{F} = \left(F_x, F_y, F_z\right), \vec{M}\left(M_x, M_y, M_z\right).$$

2. Numerical Method

The quadrilateral elements are treated by the boundary element method. First-order flat-plate theory of continous source intensity distribution and fourth-order Runge-Kutta time integration method (4RK method) are selected. In addition, the hull is divided by the fixed mesh. The non-linear superposition of the forward velocity, the stationary ship wave, diffracted wave, diffraction wave and incident wave field are considered.

1) Free Surface Formation

The free surface is generated by the hybrid Euler-Lagrangian method. In the process, the Euler method is used to solve the BVP (Boundary value problem) to obtain the velocity potential and calculate the velocity, and then carry out through the method of

iterating free surface BC (Boundary condition).

$$\vec{x}(t+dt)=\vec{x}(t)+\int_t^{t+dt}\frac{D_{\vec{x}}}{Dt}dt \tag{10}$$

$$\phi(t+dt)=\phi(t)+\int_t^{t+dt}\frac{D\phi}{Dt}dt \tag{11}$$

2) Wave Damping

In order to avoid adverse wave reflection, the damping area is set manually at the edge of the free surface. A damping term is added to the free surface boundary condition.

$$\frac{D\vec{x}}{Dt}=\nabla\phi-v\vec{x}_{damp} \tag{12}$$

$$\frac{D\phi}{Dt}=-gz+\frac{1}{2}\nabla\phi\cdot\nabla\phi-\frac{P_a}{\rho}\vec{\phi}_{damp} \tag{13}$$

where ϕ is the damping coefficient which gently increases to the boundary layer, and

$$\vec{x}_{damp}=\vec{x}_{inner}-\vec{x}_{outer}$$

$$\vec{\phi}_{damp}=\vec{\phi}_{inner}-\vec{\phi}_{outer}$$

3. Stokes Regular Wave Theory

When the finite water depth kd $\to\infty$, the first-order velocity potential, wave elevation and horizontal velocity of Stokes wave in deep water are respectively expressed as,

$$\phi=\frac{gA}{\omega}e^{kz}\sin\theta \tag{14}$$

$$\eta=A\cos\theta \tag{15}$$

$$u=\frac{gKA}{\omega}e^{kz}\cos\theta \tag{16}$$

The second-order velocity potential, wave elevation and horizontal velocity of Stokes wave in deep water are respectively expressed as,

$$\phi=\frac{gA}{\omega}e^{kz}\sin\theta \tag{17}$$

$$\eta=A\left(\cos\theta+\frac{Ak}{2}\cos2\theta\right) \tag{18}$$

$$u=\frac{kKA}{\omega}e^{kz}\cos\theta \tag{19}$$

The fifth-order velocity potential, wave elevation and horizontal velocity of Stokes wave in deep water are respectively expressed as,

$$\phi=\sqrt{\frac{g}{k_5^3}}\left(kAe^{k_5z}\sin\theta-\frac{1}{2}k_5^3A^3e^{k_5z}\sin\theta+\frac{1}{2}k_5^4A^4e^{2k_5z}\sin2\theta-\frac{37}{24}k_5^5A^5e^{k_5z}\sin\theta+\frac{1}{12}e^{3k_5z}\sin3\theta\right) \tag{20}$$

$$\eta=A\left[\left(1-\frac{3}{8}k_5^2A^2-\frac{422}{384}k_5^4A^4\right)\cos\theta+\left(\frac{1}{2}k_5A+\frac{1}{3}k_5^3A^3\right)\cos2\theta+\left(\frac{3}{8}k_5^2A^2+\frac{297}{384}\frac{1}{3}k_5^4A^4\right)\cos3\theta+\frac{1}{3}k_5^3A^3\cos4\theta+\frac{125}{384}k_5^4A^4\cos5\theta\right] \tag{21}$$

$$u=\sqrt{\frac{g}{k_5}}\left(k_5Ae^{k_5z}\cos\theta-\frac{1}{2}k_5^3A^3e^{k_5z}\cos\theta+k_5^4A^4e^{2k_5z}\cos2\theta-\frac{37}{24}k_5^5A^5e^{k_5z}\cos\theta+\frac{1}{4}e^{3k_5z}\sin3\theta\right) \tag{22}$$

where A is the amplitude, k is the wave number, ω is the wave circular frequency, $\omega=\sqrt{gk_s}\left(1+\frac{1}{2}k_5^2A^2+\frac{1}{9}k_5^4A^4\right)$, θ is the phase.

III. CALCULATION PROCESS

Firstly, offset sheet of the ship is input, coordinate system and initial position of the ship are defined; the wave type (regular wave) is selected; wave parameters (including wave height, wavelength, incidence angle and initial phase, etc.) are given; quality attributes of the ship, design speed and fluid density are defined. Then, the constraint condition is defined, the hull surface and the free surface are treated by meshing subdivision, mesh of the bow and the stern of the hull should be properly encrypted. Finally, the solution conditions are set which include the largest number of iterations, the time step and the initial free surface wave. Specific calculation process is shown in Fig. 1.

IV NUMERICAL CALCULATION AND ANALYSIS OF EXAMPLES

In this paper, the 3600 TEU container ship model of KRISO is selected as the research object. This type of ship is an international standard ship type, and the rationality of the data in this paper can be verified by referring to the data results of Gothenburg 2000, Gothenburg 2010 and other meetings. The following Table 1 gives the main parameters of the ship type.

Table. 1. Principle dimensions and ship type parameters.

	Designed waterline length (L_{wl})/m	Beam (B_{wl})/m	Deep (D)/m	Draft (d)/m	Wet surface area (S)/m^2	Square coefficient C_B	Design speed (v)/kn
Full Scale	232.5	32.2	19	10.8	9424	0.6505	24
Model Scale	4.448	0.616	0.363	0.207	3.449	0.6506	4.27

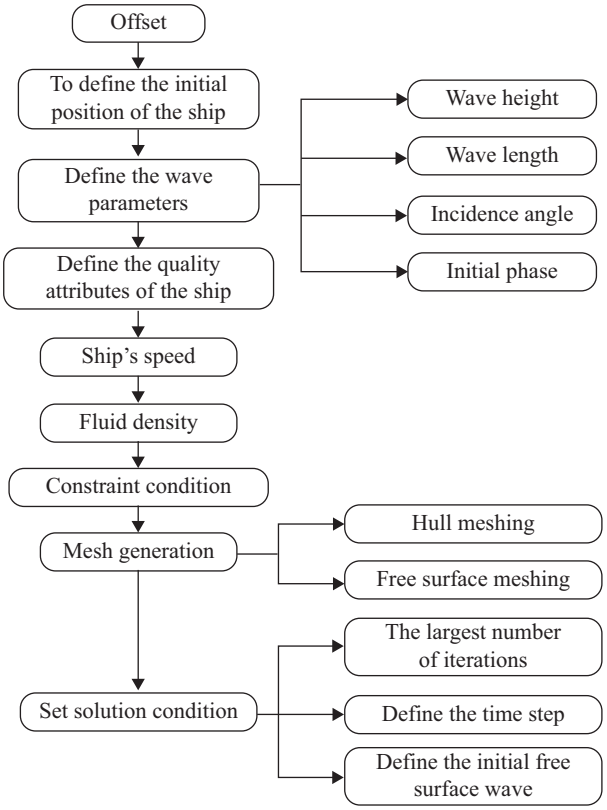

Fig. 1. Flow charts of calculation of added resistance in waves.

Fig. 2. Mesh subdivision of the hull surface element.

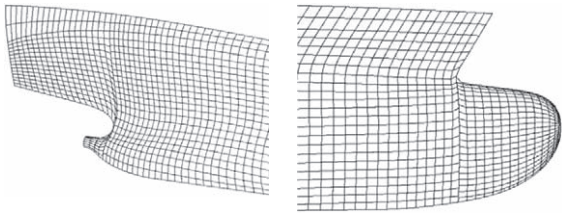

Fig. 3. Partial mesh subdivision of the bow and tail.

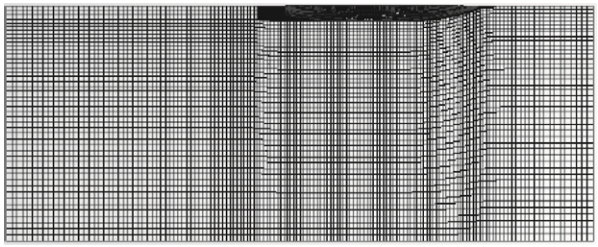

Fig. 4. Schematic diagram of the free surface mesh subdivision.

1. Computational Domain and Mesh Subdivision

The computational domain is 2.75L from the bow forward and 0.35L from the stern backward in the longitudinal direction, 0.6L laterally away in the transverse direction.

In the case of meshing, the instantaneous wet surface and the instantaneous water surface of the ship need to be divided into the surface element mesh, and mesh of the bow and the stern which have large curvature changes should be properly encrypted. In addition, the surface element mesh of free surface near the ship hull should be encrypted, and keep on uniform distribution in the longitudinal direction. In this paper, the mesh subdivision is divided into two parts: hull mesh subdivision and free surface mesh subdivision.

In order to control the mesh to ensure the rationality of the hull mesh, the hull mesh is divided into four parts: square body, bow, stern and tail shaft, as shown in Fig. 2 and Fig. 3. Square body is divided into 96 parts (stations = 96) along the length of the ship and 20 parts (points = 20) along the vertical direction equally; the bow is divided into 11 parts (stations = 11) along the longitudinal direction and 14 (points = 14) along the vertical direction equally; the tail shaft is divided into 5 parts (stations = 5) along the length of the ship and 7 parts (points = 7) along the vertical direction equally; The upper part of the stern is divided into 16 (stations = 16) along the length of the ship and 13 parts (points = 13) along the vertical direction equally.

The free surface is also divided into several sections when meshing, as the Fig 4 shows. The hull is non-dimensionalized as length of 1, thus, the X coordinates of key endpoints of the free surface are XUPS = -0.35, XBOW = 0, XSTE = 1, XDOW = 1.75485 and the Y coordinate of endpoints in the transverse direction is Y4SIDE = -0.643405. Specifically, the mesh is divided into 52 parts (points = 52) in the transverse direction. The free surface at the back of the stern is divided into 28 parts (STAU = 28), The free surface where the hull is divided into 81 points (STAM = 81), and the free surface in front of the bow is divided into 61 parts (STAD = 61).

In summary, there are 10764 surface elements and 11171 nodes in the hull and free surface.

2. Boundary Condition Setting

Using the free surface and no-slip boundary conditions, Only

Table. 2. Calculation of working conditions of head sea in regular waves.

Fr	λ/L	A_k
0.26	0.5, 1.15, 1.33, 1.5, 2	1/60

Table. 3. Calculation results of heave.

		λ/L				
		0.5	1.15	1.33	1.5	2.0
Zero order harmonic wave heaving amplitude	R3A0	-1.054E-03	-1.245E-03	-1.276E-03	-1.400E-03	-1.595E-03
First order harmonic wave heaving amplitude	R3A1	5.320E-04	8.822E-03	9.120E-03	8.574E-03	9.005E-03
Second order harmonic wave heaving amplitude	R3A2	8.658E-06	8.376E-05	5.456E-05	8.481E-05	1.465E-04
Third order harmonic wave heaving amplitude	R3A3	2.641E-06	1.198E-05	5.987E-06	2.369E-06	2.208E-06
First order harmonic wave heaving phase	R3P1	-22.137	-75.238	170.834	-45.012	74.994
Second order harmonic wave heaving phase	R3P2	59.618	-134.5	-86.310	177.441	60.598
Third order harmonic wave heaving phase	R3P3	95.383	9.012	96.734	-78.255	137.852

Table. 4. Calculation results of pitch.

		λ/L				
		0.5	1.15	1.33	1.5	2.0
Zero order harmonic wave pitching amplitude	R5A0	-4.950E-02	8.978E-03	-1.693E-02	-6.783E-02	-0.130
First order harmonic wave pitching amplitude	R5A1	0.140	2.226	2.566	2.440	1.853
Second order harmonic wave pitching amplitude	R5A2	5.277E-03	2.425E-02	3.142E-02	4.684E-02	4.409E-02
Third order harmonic wave pitching amplitude	R5A3	5.377E-04	4.428E-03	4.767E-03	6.529E-03	2.564E-03
First order harmonic wave pitching phase	R5P1	70.789	-37.840	-150.886	3.572	146.841
Second order harmonic wave pitching phase	R5P2	61.880	-135.274	-87.276	-151.924	119.046
Third order harmonic wave pitching phase	R5P3	-134.312	48.694	109.450	-119.240	-25.975

consider two degrees of freedom, pitch and heave, and restrict four degrees of freedom, surge, sway, roll and yaw.

3. Calculation of Working Conditions

In this paper, Used Shipflow software and self-compiled program to calculate the seakeeping ability of the ship at the speed of Fr = 0.26 in regular head waves of the λ/L = 0.5~2 and A_K = 1/60, specific calculation of working conditions are shown in the following Table 2.

V. ANALYSIS OF CALCULATION RESULTS

1. Calculation Results of Ship Heave and Pitch in Head Sea

The motion expressions of heave and pitch of the hull in the regular head sea are expressed as:

$$z = z_a \cdot \cos\left(\omega_e t + \varepsilon_z\right) \tag{23}$$

$$\theta = \theta_a \cdot \cos\left(\omega_e t + \varepsilon_v\right) \tag{24}$$

where ω_e is the encounter frequency of ship model, z_a and θ_a are heave amplitude and pitch amplitude respectively, ε_z and ε_v are heave phase and pitch phase respectively.

Table 3 and Table 4 show each order calculation results of amplitude and phase of heave and pitch respectively, which are in five typical conditions with wave length-ship length ratio of 0.5, 1.15, 1.33, 1.5 and 2.0.

The dimensionless amplitude of heave and pitch motions are expressed as:

$$z_a'' = \frac{z_a}{A} \tag{25}$$

$$\theta_a'' = \frac{\theta_a}{KA} \tag{26}$$

The heave amplitude z_α and pitch amplitude θ_α in the calculation of dimensionless amplitude of heave and pitch motions are R3A1 and R5A1 respectively. In the calculation of Shipflow software, the length of the ship is dimensionless to 1. In order to verify the accuracy of numerical results, Fig. 5 is the dimensionless amplitude curve of the heave motion with different wave length-ship length ration. It can be seen from the figure that numerical calculation results fit well with experimental results, the two trends are similar and the values are approaching.

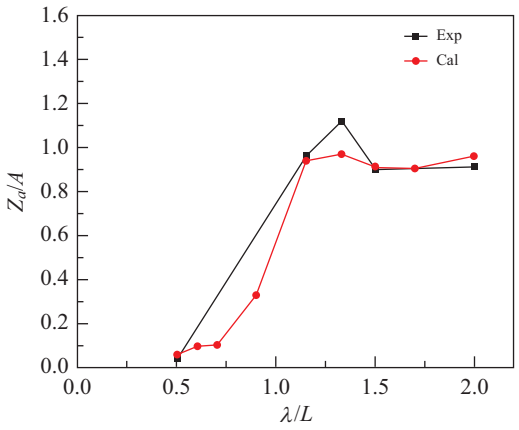

Fig. 5. Dimensionless amplitude curve of heave.

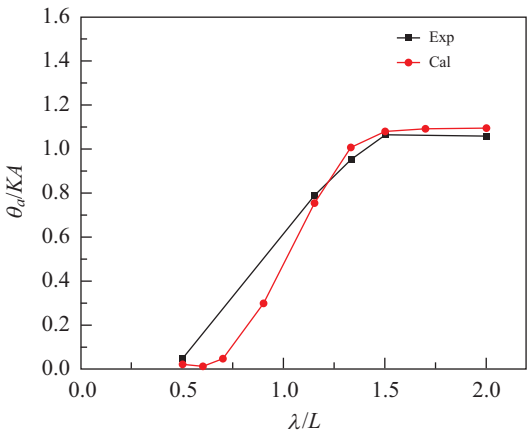

Fig. 6. Dimensionless amplitude curve of pitch.

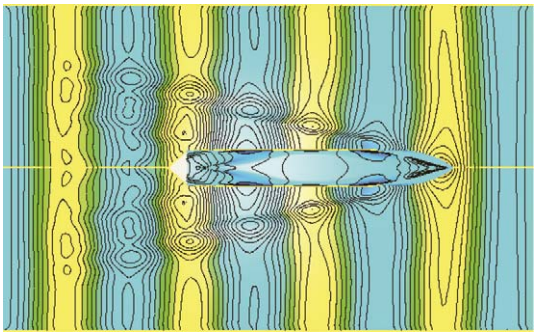

Fig. 7. λ/L = 0.5 α_k =1/60 wave pattern.

The problems is that numerical calculation result is lower than experimental result with the wave length-ship length ratio of 1.33 and don't reach the ideal peak value. Fig. 6 is the dimensionless amplitude curve of the pitch motion with different wave length-ship length ratio. As the figure shows, numerical calculation results are almost same as experimental results. Since there are only two endpoints experimental values with the wave length-ship length ratio of 0.5 to 1.15, numerical calculation results of

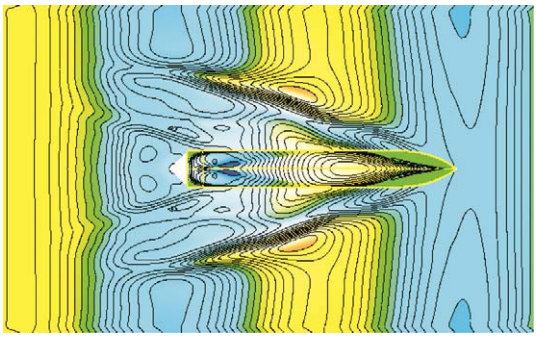

Fig. 8. λ/L = 1.15 α_k = 1/60 wave pattern.

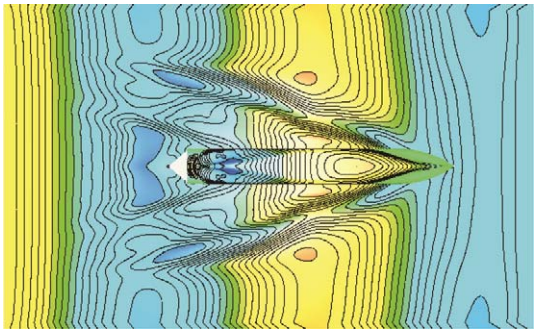

Fig. 9. λ/L = 1.33 α_k = 1/60 wave pattern.

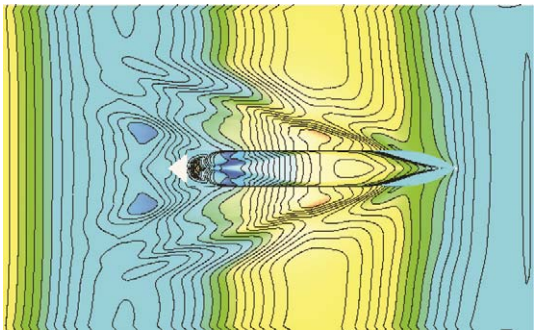

Fig. 10. λ/L = 1.5 α_k = 1/60 wave pattern.

three points with the wave length-ship length ratio of 0.6, 0.7 and 0.9 do not fit well with the curve of experimental results.

2. Wave Pattern

Figs. 7-10 are four representative wave patterns of free surface with wave length-ship length ratio of 0.5, 1.15, 1.33 and 1.5. The interaction between waves and ship hull can be seen from the wave pattern, and smooth area at the back of free surface can also reflect the effectiveness of wave damping in numerical simulation.

3. Calculation Results of Added Resistance in Head Sea

Table 5 shows each order calculation results of amplitude and phase of added resistance, which is in five typical conditions with wave length-ship length ratio of 0.5, 1.15, 1.33, 1.5 and 2.0.

Table. 5. Calculation results of added wave resistance.

		λ/L				
		0.5	1.15	1.33	1.5	2.0
Zero order harmonic wave added resistance amplitude	F1A0	8.574E-06	2.014E-05	1.654E-05	1.168E-05	6.161E-06
First order harmonic wave added resistance amplitude	F1A1	2.603E-05	2.084E-05	5.693E-05	7.628E-05	8.679E-05
Second order harmonic wave added resistance amplitude	F1A2	6.572E-06	1.038E-05	1.006E-05	6.162E-06	2.075E-06
Third order harmonic wave added resistance amplitude	F1A3	1.150E-06	1.023E-05	5.402E-06	2.218E-06	4.739E-07
First order harmonic wave added resistance phase	F1P1	-100.513	-6.908	-135.405	17.628	158.812
Second order harmonic wave added resistance phase	F1P2	-109.196	-53.868	62.027	14.476	-14.262
Third order harmonic wave added resistance phase	F1P3	169.968	-172.194	-163.737	-90.392	-78.118

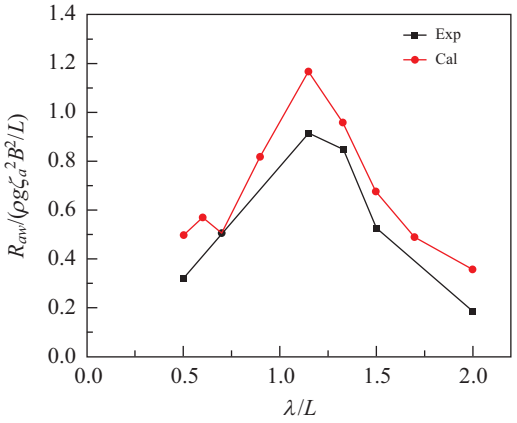

Fig. 11. Frequency response curves of added resistance with different wave length-ship length ratio.

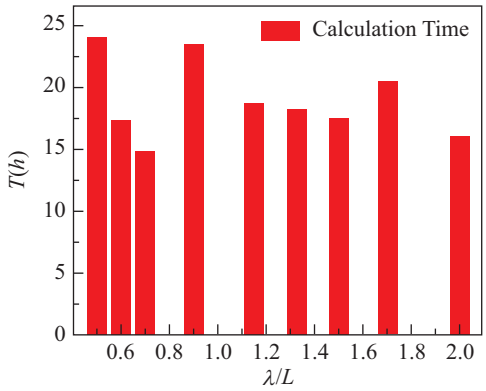

Fig. 12. Statistical chart of calculation time.

The calculation formula of transfer function of dimensionless added resistance is expressed as:

$$r_{aw} = \frac{R_{aw}}{\rho g \zeta_a^2 B^2 / L_{PP}} \tag{27}$$

Where, R_{aw} is added resistance in regular waves, ρ is the density, g is the acceleration of gravity, ζ_a is amplitude of regular wave, B is the beam, L_{pp} is the length between perpendiculars.

Fig. 11 shows the comparison between numerical results of dimensionless added resistance in head sea and experimental results at the speed of $Fr = 0.26$. It can be seen from the figure that the general trend of numerical results and experimental results are consistent, but the numerical results are slightly higher than the experimental results. In addition, the peak position of the two are similar with wave length-ship length ratio of 1.15, which is very reasonable. Generally speaking, the results obtained in this paper are not as accurate as those obtained by viscous flow method, however, the results are generally acceptable.

4. Time Statistics of Numerical Computation

The accuracy of three-dimensional fully nonlinear time-domain potential flow theory is improved comparing with strip theory, but it is lower than the viscous flow method. However, in the case of calculation error is acceptable, the three-dimensional fully nonlinear time-domain potential flow method has advantage of shorter computation time when it is compared with the viscous flow method which needs a long time to calculate. In this paper, computing hardware is a laptop with 4G memory, setting the thread count of calculation to 6. It can be seen clearly from Fig. 12 that average computation time in regular head waves with different wave length-ship length ratio is about 19 h by the method. And combining with previous analysis, the nonlinear time-domain potential flow theory is also a more accurate and efficient analysis method.

5. Calculation of Added Resistance in Different Wind Direction Angles

On the basis of head sea, the added resistance in different wind direction angles is further discussed in five conditions with wave length-ship length ratio of 0.5, 1.15, 1.33, 1.5 and 2.0. Wind direction angles are 0 degrees, 45 degrees, 90 degrees, 135 degrees and 180 degrees respectively. Curves of heave amplitude, pitch amplitude and added resistance in different wind direction angles are given in Figs. 13-15.

It can be seen from dimensionless amplitude curves of heave motion and pitch motion in Fig. 13 and Fig. 14, the numerical results in wind direction angle of 180 degrees have been compared with the experimental results previously, and the trend of amplitude curves of heave and pitch in the other wind direction angles are basically the same as in head sea apart from

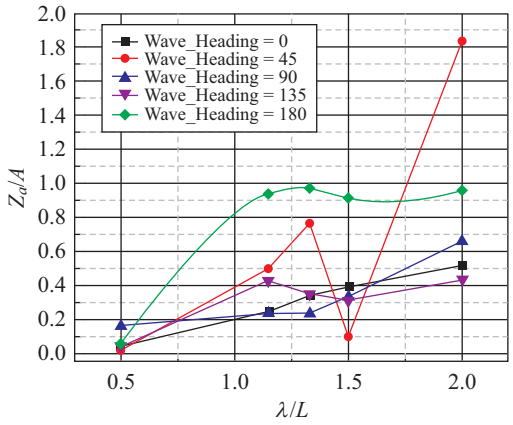

Fig. 13. Dimensionless amplitude curves of heave motion in different wind direction angles.

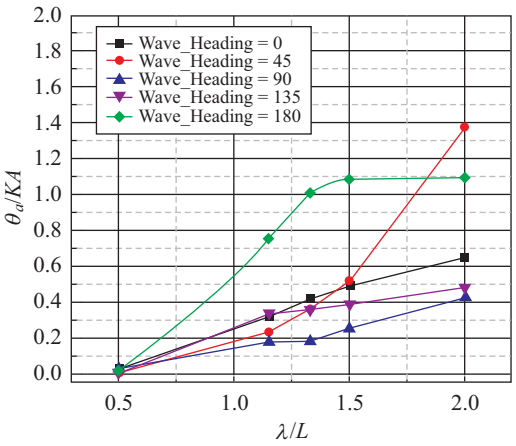

Fig. 14. Dimensionless amplitude curves of pitch motion in different wind direction angles.

the case of wind direction angle of 45 degrees, but the amplitude is less than that in head sea. Unfortunately, the results of wind direction angle of 45 degrees are not satisfactory, which remain to be further explored. As it can be seen from dimensionless curves of added resistance in Fig. 15, all values of added resistance in head sea are higher than conditions in the other wind direction angles with wave length-ship length ratio of 0.5, 1.15, 1.33, 1.5 and 2.0.

VI. CONCLUSION

In this paper, the added resistance of KCS ship in regular waves is calculated based on the three-dimensional fully nonlinear time-domain potential flow theory. The added resistance of KCS ship at the service speed of $Fr = 0.26$ in regular head waves of the $\lambda/L = 0.5$~2 is researched. In the calculation process, only consider two degrees of freedom, pitch and heave, and restrict four degrees of freedom, surge, sway, roll and yaw. It can be found that calculation results obtained by this method are more ideal by comparing with experimental results, and com-

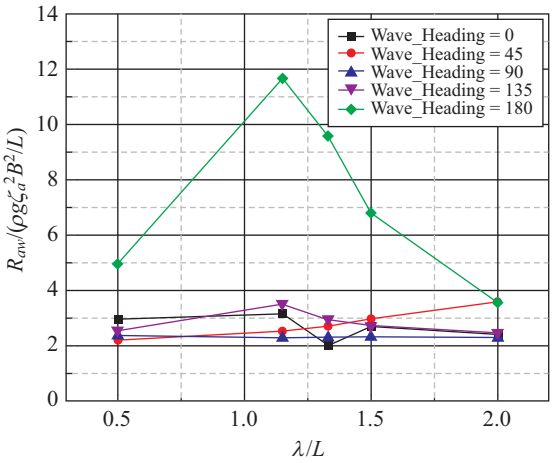

Fig. 15. Dimensionless curves of added resistance in different wind direction angles.

putation time is shorter than viscous flow method. Considering the factors of accuracy and efficiency, the three-dimensional fully nonlinear time-domain potential flow theory is a good calculation method.

Furthermore, the results of heave, pitch and added resistance with different wind direction angles and wave length-ship length ratio are studied. The numerical simulation results in wind direction angle of 180 degrees have been compared with the experimental results previously to verify its accuracy. The trend of amplitude curves of heave and pitch in the other wind direction angles are basically the same as in head sea apart from the case of wind direction angle of 45 degrees, but the amplitude is less than that in head sea. Unfortunately, the results of wind direction angle of 45 degrees are not satisfactory, which remain to be further explored. And all values of added resistance in head sea are higher than conditions in the other wind direction angles with wave length-ship length ratio of 0.5, 1.15, 1.33, 1.5 and 2.0.

ACKNOWLDEGEMENTS

Foundation item: Supported by National P & D Program of China (No.2016YFB0300700, 2016YF0300704), National Natural Science Foundation of China (No. 51779135, 51009087), Shanghai Natural Science Foundation of China (project approval number: 14ZR1419500).

REFERENCES

Duan, W. Y., R. F. Wang, W. X. Ma and S. Ma (2014). Numerical methods investigation on added resistance of high speed ship in waves. Journal of Ship Mechanics 18, 1175 -1183.

Deng, X. H., Z. Z. Fang and B. Q. Zhao (2015). Automated optimization of the ship hull form with minimum resistance based on CFD. Chinese Journal of Ship Research 10(3),19-25.

Fang, Z. Z., R. C. Zhu, G. P. Miao and X. H. Yang (2012). Numerical calculation of hydrodynamic forces for a ship in regular waves based on numerical wave tank. Chinese Journal of Hydrodynamics 27, 515-524.

Jin, H. Z., Z. Q. Liu and S. Q. Jiang (2013). Relationship between ship roll attitude and added resistance. Journal of applied sciences-electronics and information engineering 31,309-314

Kim, K. H. and Y. Kim (2011). Numerical study on added resistance of ships by using a time-domain Rankine panel method. Ocean Engineering 38, 1357-1367.

Li, J. P., G. X. Dong, Y. X. Jiang and H. H. He (2012). The study of the added resistance in waves of the ship and the influence of the headline. Journal of shanghai ship and shipping research institute 35, 34-38.

Park, D. M., J. Lee and Y. H. Kim (2015). Uncertainty analysis for added resistance experiment of KVLCC2 ship. Ocean Engineering 95, 143-156.

Shen, Z. R., H. X. Ye and D. C. Wan (2012). Motion response and added resistance of a ship in head waves based on RANS simulations. Chinese journal of hydrodynamics 27,621-633.

Seo, M. G., D. M. Park, K. K. Yang and Y. Kim (2013). Comparative study on computation of ship added resistance in waves. Ocean Engineering 73, 1-15.

Xie, Y. P., W. Yao, C. J. Mi and X. P. Zhang (2013). Numerical Wave tank and computation of added resistance for displacement high speed craft in regular waves. Ship Engineering 35,5-8.

Xie, Y. P., S. S. Yuan, X. S. Xu and D. F. Hu (2017). Asymmetric catamaran hull configuration and the relevant research of resistance performance. Ship science and technology 39(8), 28-46.

Zhang, B. J. (2011). Research on optimization design of the full-hull lines for reducing resistance in still water and added resistance in waves. Journal of Huazhong university of science and technology (Natural science edition) 9, 32-35.